

Probing the Scotogenic Dirac Model with FIMP Dark Matter and ΔN_{eff} *

Shu-Yuan Guo (郭书源)[†] Man-Yu Zhao (赵曼玉)[‡]

Department of Physics, Yantai University, Yantai 264005, China

Abstract: We study a feebly interacting massive particle realization of the Scotogenic Dirac Model in which the lightest neutral fermion N_1 serves as a dark matter candidate, produced via the freeze-in or super-WIMP mechanism. The model generates Dirac neutrino masses at one loop, resulting in a rank-2 mass matrix that predicts one nearly massless neutrino. We analyze the DM relic density for various next-to-lightest odd particles (NLOPs), finding that coannihilation effects and enhanced annihilation channels are crucial for achieving the correct thermal freeze-out abundance of the NLOP. We provide a detailed analysis of the model's implications for the effective number of relativistic species, ΔN_{eff} , which receives contributions from both a thermal bath of right-handed neutrinos and non-thermal energy injection due to late NLOP decays. Through an extensive parameter scan, we identify viable parameter space for all NLOP candidates that satisfies constraints from DM relic density, lepton flavor violation, Big Bang Nucleosynthesis, Cosmic Microwave Background, and ΔN_{eff} .

Keywords: neutrino mass, dark matter, neutrino cosmology

DOI: **CSTR:**

I. INTRODUCTION

The phenomenon of neutrino oscillations [1–6] provides strong evidence that neutrinos must have non-zero masses. For neutral fermions such as neutrinos, two types of mass are theoretically possible: Dirac and Majorana. On the experimental front, extensive efforts have been devoted to searching for lepton number violation—a featured signature of Majorana neutrinos. Experiments at colliders [7, 8] and neutrinoless-double-beta-decay ($0\nu\beta\beta$) [9–14] searches, in particular, have so far yielded no positive signals. As a result, the alternative scenario has received increasing attention in recent years [15–54]. To generate the tiny Dirac neutrino masses, an attractive approach is to attribute them to a radiative mechanism realized through loop diagrams. The loop suppression naturally explains the smallness of the masses, while the particles running in the loop can carry quantum numbers under a discrete symmetry. This same symmetry can stabilize the lightest particle in the loop, making it a viable dark matter (DM) candidate.

The weakly interacting massive particle (WIMP) paradigm, featuring electroweak-scale particles with weak cross sections ($\sigma \sim 10^{-26} \text{ cm}^2/\text{s}$), naturally yields

the observed DM density ($\Omega_{\text{DM}} h^2 \approx 0.12$) via thermal freeze-out (see [55] for a review). However, this paradigm faces significant challenges from null results in DM direct detection [56, 57]. In response, the feebly interacting massive particle (FIMP) scenario has emerged as a compelling alternative [58–62]. Unlike thermal WIMPs, FIMPs are produced via extremely weak couplings, avoiding current experimental bounds while naturally explaining the observed dark matter abundance.

The Scotogenic Dirac Model, originally proposed in Ref. [20] and later developed with an alternative symmetry realization in Ref. [63], extends the SM with right-handed neutrinos ν_R , vector-like fermions N , a scalar doublet Φ , and a scalar singlet χ . Previous work in Ref. [63] explored the scenario where the lightest fermion N_1 acts as a WIMP dark matter. This scenario faces significant challenges due to stringent constraints from lepton flavor violation (LFV) experiments, which severely limit the Yukawa couplings required for efficient thermal relic production. Consequently, achieving the observed relic density requires substantial tuning of parameters and relies on annihilation channels mediated by the y_χ coupling. In this work, we propose a novel realization of the Scoto-

Received 25 August 2025; Accepted 3 November 2025

* This work by S.-Y.G. was supported by the NNSFC under Grant No. 12305113, by the Natural Science Foundation of Shandong Province under Grants No. ZR2022QA026, and by the Project of Shandong Province Higher Educational Science and Technology Program under Grants No. 2022KJ271

[†] E-mail: shyuanguo@ytu.edu.cn

[‡] E-mail: manyuzhao@s.ytu.edu.cn



Content from this work may be used under the terms of the Creative Commons Attribution 3.0 licence. Any further distribution of this work must maintain attribution to the author(s) and the title of the work, journal citation and DOI. Article funded by SCOAP³ and published under licence by Chinese Physical Society and the Institute of High Energy Physics of the Chinese Academy of Sciences and the Institute of Modern Physics of the Chinese Academy of Sciences and IOP Publishing Ltd

genic Dirac Model in which the lightest neutral fermion N_1 serves as a FIMP DM candidate. This scenario is defined by the extreme suppression of the Yukawa couplings $(y_\Phi)_{\alpha 1}$ and $(y_\chi)_{\alpha 1}$, which ensures that N_1 never enters thermal equilibrium with the Standard Model (SM) plasma throughout cosmic history. This FIMP framework not only provides a natural mechanism for DM production but also has a profound impact on neutrino physics, leading to a rank-2 structure for the neutrino mass matrix. This structure predicts one nearly massless neutrino state, which is allowed by the oscillation data. We systematically investigate two complementary production mechanisms for N_1 . The first is the conventional freeze-in mechanism, where N_1 is slowly produced via the extremely small Yukawa couplings through decays of heavier Z_2 -odd scalars and fermions. The second is the super-WIMP mechanism, where N_1 is produced by the late decays of a thermally frozen-out next-to-lightest odd particle (NLOP). The identity of the NLOP—whether it is N_2 , $\phi_{R,I}$, ϕ^\pm , or χ —plays a crucial role in shaping the model's phenomenology, directly influencing the DM relic abundance and cosmological observables. A central focus of our analysis is the effective number of relativistic species, ΔN_{eff} . We show that the deviation ΔN_{eff} receives contributions from two distinct sources: a thermal component from the primordial bath of right-handed neutrinos, and a non-thermal component arising from energy injection due to late NLOP decays. Our comprehensive parameter scan demonstrates that viable regions of parameter space exist for all possible NLOP candidates, satisfying all current observational constraints from DM relic density, lepton flavor violation, BBN, CMB, and ΔN_{eff} .

The remainder of this paper is organized as follows: Section II introduces the FIMP Scotogenic Dirac Model and the mechanism for Dirac neutrino mass generation. Section III details the dark matter relic density calculations. Section IV analyzes the cosmological implications for the effective number of relativistic species. Finally, we make our conclusion in Section V.

II. THE MODEL

The Scotogenic Dirac Model was originally proposed in Ref. [20], and a different symmetry realization was put forward in [63] by one of the authors. In Table 1 we list out the relevant particles in this model. Apart from the Standard Model lepton doublet $F_L = (\nu_L, \ell_L)^T$ and Higgs H , additional species are the right-handed neutrinos ν_R , three vector-like fermions N , an extra scalar doublet $\Phi \equiv (\phi^+, (\phi_R + i\phi_I)/\sqrt{2})^T$ and scalar singlet χ . Tree-level Dirac neutrino masses and possible Majorana masses of ν_R and N are forbidden due to the existence of Z_3 .

The introduction of new particles in Table 1 would bring in the following interactions:

Table 1. Particles and symmetries in the scotogenic Dirac model.

	F_L	H	ν_R	N	Φ	χ
$SU(2)_L$	2	2	1	1	2	1
$U(1)_Y$	-1/2	1/2	0	0	1/2	0
Z_3	0	0	ω	ω	ω	0
Z_2	+	+	+	-	-	-

$$-\mathcal{L}_{\text{new}} \supset (y_\Phi \bar{F}_L \tilde{\Phi} N + y_\chi \bar{\nu}_R \chi N + \text{h.c.}) + m_N \bar{N} N, \quad (1)$$

where $\tilde{\Phi} \equiv i\sigma_2 \Phi^*$. Relevant scalar potential terms are given by

$$\begin{aligned} V = & -\mu_H^2 H^\dagger H + \mu_\Phi^2 \Phi^\dagger \Phi + \frac{1}{2} \mu_\chi^2 \chi^2 + \frac{1}{2} \lambda_1 (H^\dagger H)^2 \\ & + \frac{1}{2} \lambda_2 (\Phi^\dagger \Phi)^2 + \frac{1}{4!} \lambda_3 \chi^4 \\ & + \lambda_4 (H^\dagger H)(\Phi^\dagger \Phi) + \frac{1}{2} \lambda_5 (H^\dagger H) \chi^2 \\ & + \frac{1}{2} \lambda_6 (\Phi^\dagger \Phi) \chi^2 + \lambda_7 (H^\dagger \Phi)(\Phi^\dagger H) \\ & + (\mu \Phi^\dagger H \chi + \text{h.c.}). \end{aligned} \quad (2)$$

The scalar singlet χ is set as real, for simplicity. The μ -terms in Eq. (2) is the source which softly break the Z_3 symmetry, hence it's natural to keep it a small value. The one-loop neutrino mass (as illustrated in Fig. 1) is then generated as

$$\begin{aligned} (M_\nu)_{\alpha\beta} = & \frac{\sin 2\theta}{32\pi^2 \sqrt{2}} \sum_{k=1,2,3} (y_\Phi)_{\alpha k} (y_\chi^*)_{\beta k} m_{N_k} \\ & \times \left(\frac{m_1^2}{m_1^2 - m_{N_k}^2} \ln \frac{m_1^2}{m_{N_k}^2} - \frac{m_2^2}{m_2^2 - m_{N_k}^2} \ln \frac{m_2^2}{m_{N_k}^2} \right). \end{aligned} \quad (3)$$

Lower indices $\alpha(\beta)$ and k stand for different generations of leptons and N s. The angle θ in Eq. 3 originates from mixing between the real component of scalar doublet Φ and singlet χ . When the SM Higgs H acquires its vacuum expectation value v after electroweak spontaneous symmetry breaking, the angle is quantitatively fixed as

$$\tan 2\theta = \frac{2\sqrt{2}\mu v}{\mu_\Phi^2 - \mu_\chi^2 + (\lambda_4 - \lambda_5)v^2}. \quad (4)$$

The $m_{1(2)}^2$ in Eq. 3 indicate eigenvalues of the $\chi - \phi_R$ mixing mass-square matrix

$$m_{(\chi, \phi_R)}^2 = \begin{pmatrix} \mu_\chi^2 + \lambda_5 v^2 & \sqrt{2}\mu v \\ \sqrt{2}\mu v & \mu_\Phi^2 + (\lambda_4 + \lambda_7)v^2 \end{pmatrix}. \quad (5)$$

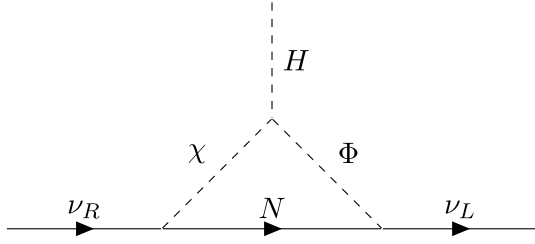


Fig. 1. The one-loop neutrino mass in Scotogenic Dirac Model.

Treating μ as a tiny parameter results in small mixing, justifying the approximation $m_{1(2)} \approx m_{\chi(\phi_R)}$. Hence we will use m_χ and m_{ϕ_R} hereafter. The masses of the other scalars are $m_h^2 = 2\lambda_1 v^2$, $m_{\phi^\pm}^2 = \mu_\phi^2 + \lambda_4 v^2$, $m_{\phi_1}^2 = \mu_\phi^2 + (\lambda_4 + \lambda_7)v^2$. Here h is the observed 125 GeV boson.

The assignment of Z_2 in Table 1 would make particles in loop of Fig. 1 to be in dark-sector, and the lightest one is naturally served as the dark matter particle candidate. In Ref. [63], we had made a detailed study on the situation that N_1 is a WIMP-type dark matter particle. In this work, however, we explore an alternative scenario where the dark matter candidate N_1 is a feebly interacting massive particle. The FIMP nature of N_1 implies that the Yukawa couplings $(y_\Phi)_{\alpha 1}$ and $(y_\chi)_{\alpha 1}$ are extremely small. This setup significantly distinguishes the model from the conventional WIMP Dirac scotogenic framework. From Eq. 3, we observe that the neutrino mass matrix M_ν is approximately of rank-2, a direct consequence of the suppressed couplings $(y_\Phi)_{\alpha 1}$ and $(y_\chi)_{\alpha 1}$. This structure predicts that one of the three neutrino mass eigenstates is nearly massless, which remains consistent with the oscillation data requiring at least two massive neutrinos.

The Yukawa interactions y_Φ could mediate processes leading to LFV, which is extremely suppressed in SM. On the experimental side, the most stringent limits arise from the rare decays $\ell_\alpha \rightarrow \ell_\beta \gamma$. The decay branching ratio is calculated as

$$\text{Br}(\ell_\alpha \rightarrow \ell_\beta \gamma) = \text{Br}(\ell_\alpha \rightarrow \ell_\beta \nu_\alpha \bar{\nu}_\beta) \times \frac{3\alpha_{\text{em}}}{16\pi G_F^2} \left| \sum_i \frac{(y_\Phi)_{\beta i} (y_\Phi^*)_{\alpha i}}{m_{\phi^\pm}^2} j \left(\frac{m_{N_i}^2}{m_{\phi^\pm}^2} \right) \right|^2, \quad (6)$$

here $j(r) = (1 - 6r + 3r^2 + 2r^3 - 6r^2 \ln r) / (12(1 - r)^4)$. The latest result from MEG II reported the limit as $\text{Br}(\mu \rightarrow e \gamma) \lesssim 1.5 \times 10^{-13}$ [64]. This could be translated into limit on y_Φ as $(y_\Phi)_{\alpha 2,3} \lesssim 0.01$, if we assume the new masses are not far away from the electroweak scale. When combined with the neutrino mass in Eq. 3, and noting that the mixing angle θ is small (as it reflects the Z_3 -breaking parameter μ in Eq. 4), we deduce that $(y_\chi)_{\alpha 2,3}$ must be comparable to or larger than $(y_\Phi)_{\alpha 2,3}$. For example, with $\sin 2\theta \sim 10^{-5}$ and $(y_\Phi)_{\alpha 2,3} \lesssim 0.01$, reproducing the observed neutrino masses requires $(y_\chi)_{\alpha 2,3} \gtrsim 0.01$.

III. DARK MATTER RELIC DENSITY

The residual Z_2 symmetry confines loop particles to the dark sector, with the lightest Z_2 -odd particle serving as dark matter candidate. In [63], we analyzed the scenario where the fermion N_1 acts as WIMP dark matter. We found that the dark matter annihilation via y_Φ is difficult to achieve at the correct relic density. This limitation arises because the Yukawa coupling y_Φ faces stringent constraints from LFV. The y_Φ compatible with these LFV constraints substantially suppresses N_1 annihilation cross-sections, resulting in dark matter overproduction that is excluded by cosmological observations. Consequently, the dominant annihilation must proceed through y_χ .

In this work, however, we would try a FIMP realization of dark matter N_1 . The feeble interaction strength would retain N_1 always out of equilibrium. Thus the key ways to produce N_1 are decays of heavier Z_2 -odd particles. The dominant contributions are from decays of scalars:

$$\Gamma_{\phi_{R,I} \rightarrow N_1 \bar{\nu}_\alpha} = \frac{|(y_\Phi)_{\alpha 1}|^2}{32\pi} \frac{(m_{\phi_{R,I}}^2 - m_{N_1}^2)^2}{m_{\phi_{R,I}}^3}, \quad (7)$$

$$\Gamma_{\phi^\pm \rightarrow N_1 \ell_\alpha^\pm} = \frac{|(y_\Phi)_{\alpha 1}|^2}{16\pi} \frac{(m_{\phi^\pm}^2 - m_{N_1}^2)^2}{m_{\phi^\pm}^3}, \quad (8)$$

$$\Gamma_{\chi \rightarrow N_1 \bar{\nu}_\alpha} = \frac{|(y_\chi)_{\alpha 1}|^2}{16\pi} \frac{(m_\chi^2 - m_{N_1}^2)^2}{m_\chi^3}. \quad (9)$$

Additional production channels involve decays from $N_{2,3}$:

$$\Gamma_{N_{2,3} \rightarrow N_1 \ell_\alpha^- \ell_\beta^+} = \frac{|(y_\Phi)_{\beta 1}|^2 |(y_\Phi)_{\alpha 2,3}|^2}{6144\pi^3} \frac{m_{N_{2,3}}^3 (m_{N_{2,3}}^2 - 2m_{N_1}^2)}{m_{\phi^\pm}^4}, \quad (10)$$

$$\Gamma_{N_{2,3} \rightarrow N_1 \nu_\alpha \bar{\nu}_\beta} = \frac{m_{N_{2,3}}^3 (m_{N_{2,3}}^2 - 2m_{N_1}^2)}{6144\pi^3} \times \left(\sum_{\phi_R, \phi_1} \frac{|(y_\Phi)_{\beta 1}|^2 |(y_\Phi)_{\alpha 2,3}|^2}{m_\phi^4} + \frac{|(y_\chi)_{\beta 1}|^2 |(y_\chi)_{\alpha 2,3}|^2}{m_\chi^4} \right). \quad (11)$$

Fermionic decay contributions remain subdominant due to both three-body phase space suppression and additional Yukawa coupling factors. Moreover, decays into \bar{N}_1 and decays of $\bar{N}_2 \rightarrow N_1 (\bar{N}_1)$, whose widths are similar as in Eqns. 7 to 11, should also be taken into account to get the total abundance of dark matter. To ensure N_1 remains out of thermal equilibrium, the decay rate should be smaller than the Hubble expansion rate. A rough estimate requires the Yukawa coupling $(y_{\Phi,\chi})_{\alpha 1} \lesssim 10^{-7}$, for scalar

masses at $O(\text{TeV})$.

The evolution of dark matter and relevant particles are governed by the following Boltzmann equations:

$$\frac{dY_{N_1+\bar{N}_1}}{dz} = k^* z \sum_X (\tilde{\Gamma}_{X \rightarrow N_1} + \tilde{\Gamma}_{X \rightarrow \bar{N}_1}) Y_X, \quad (12)$$

$$\begin{aligned} \frac{dY_X}{dz} = & k^* z \sum_A \tilde{\Gamma}_{A \rightarrow X} \left(Y_A - \frac{Y_A^{\text{eq}}}{Y_X^{\text{eq}}} Y_X \right) \\ & - k^* z \sum_B \tilde{\Gamma}_{X \rightarrow B} \left(Y_X - \frac{Y_X^{\text{eq}}}{Y_B^{\text{eq}}} Y_B \right) \\ & + \frac{k}{z^2} \langle \sigma v \rangle_{\text{SM} \rightarrow X\bar{X}} \left((Y_{\text{SM}}^{\text{eq}})^2 - \frac{(Y_{\text{SM}}^{\text{eq}})^2}{(Y_X^{\text{eq}})^2} Y_X Y_{\bar{X}} \right). \end{aligned} \quad (13)$$

Here $X = \phi_R, \phi_I, \phi^\pm, \chi, N_{2,3}(\bar{N}_{2,3})$ stands for all the Z_2 -odd particles that could decay into dark matter. For a specific X , its evolution is affected by three kinds of processes: decays of heavier A into X , decays of X into lighter B , and SM pairs annihilating into X pairs. The dimensionless parameter z is defined as the ratio of the dark matter mass to the evolution temperature, i.e. $z \equiv m_{N_1}/T$. The parameter k^* is given by $k^* = \sqrt{45/(4\pi^3 g^*)} M_{\text{Pl}}/m_{N_1}^2$, g^* is the effective number of degrees of freedom of the relativistic particles, $M_{\text{Pl}} = 1.2 \times 10^{19} \text{ GeV}$ is the Planck mass. Thermal decay width $\tilde{\Gamma}_{i \rightarrow j}$ is defined as $\tilde{\Gamma}_{i \rightarrow j} = \Gamma_{i \rightarrow j} K_1/K_2$, where K_1 and K_2 denote the first and second order of modified Bessel functions of the second kind, respectively. Y_i^{eq} represents the abundance in equilibrium for species i .

In practice, we write down the model using FeynRules [65] and the output model files are used to calculate relic density by micrOmegas [66]. We present the results of this calculation in Fig. 2, which illustrates the comoving yield of N_1 as a function of the cosmological variable $z = m_{N_1}/T$ for several benchmark values of the feeble Yukawa couplings $(y_\Phi)_{\alpha 1}$ and $(y_\chi)_{\alpha 1}$. For simplicity in this analysis, we set these couplings to be equal, i.e., $(y_\Phi)_{\alpha 1} = (y_\chi)_{\alpha 1}$, while the remaining model parameters are fixed to the values specified in Table 2. The resulting evolution curves exhibit the characteristic hallmark of the freeze-in mechanism. At high temperatures

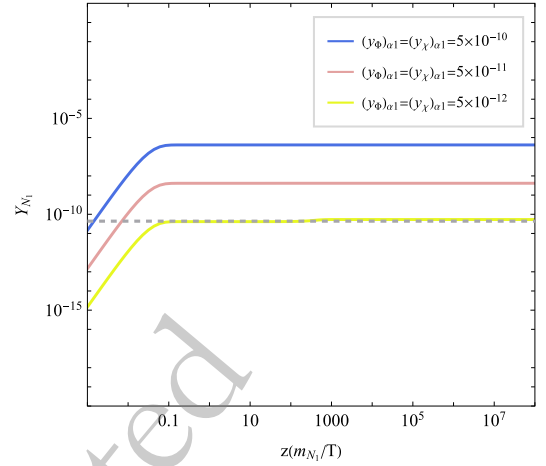


Fig. 2. (color online) The evolution of dark matter through freeze-in. The parameters used are listed in Table 2.

($z \ll 1$), the abundance of N_1 is negligible. As the universe cools, N_1 is slowly but steadily produced from decays of the heavier Z_2 -odd particles. The yield grows progressively until the source particles become thermally suppressed and depleted, at which point the comoving number density of N_1 "freezes in" and remains constant. For reference, the observed dark matter relic density, $\Omega_{\text{DM}} h^2 \approx 0.12$, is indicated by a horizontal dashed line. We demonstrate a viable parameter point, corresponding to the specific coupling strength $(y_\Phi)_{\alpha 1} = (y_\chi)_{\alpha 1} = 5 \times 10^{-12}$, successfully saturates the observed dark matter density.

In addition to the conventional freeze-in mechanism, dark matter can also be produced via the late decay of a thermally frozen-out next-to-lightest odd particle (NLOP), a scenario known as the "super-WIMP" mechanism [67]. In this framework, heavier Z_2 -odd particles decay predominantly into the NLOP in the early universe, as these transitions are not suppressed by small couplings. The NLOP is initially in thermal equilibrium with both SM and other Z_2 -odd particles, but as the universe cools, its interaction rate drops below the Hubble expansion rate, leading to decoupling and the freeze-out of its comoving number density. Subsequently, the NLOP undergoes a highly suppressed decay into the stable dark matter, due to an extremely weak coupling. This results in a long-lived NLOP and a delayed, non-thermal production

Table 2. Parameter sets used in Fig. 2 and Fig. 3, masses are given in GeV.

m_{N_1}	m_{N_2}	m_{N_3}	m_{ϕ_R}	m_{ϕ_I, ϕ^\pm}	m_χ	$(y_{\Phi, \chi})_{\alpha 1}$	$(y_\Phi)_{\alpha 2,3}$	$(y_\chi)_{\alpha 2,3}$	λ_5	Figure
10	800	800	800	800	800	$5 \times 10^{-10, -11, -12}$	10^{-3}	10^{-2}	10^{-3}	Fig. 2
10	600/770	800	800	800	800	5×10^{-13}	10^{-2}	10^{-2}	10^{-3}	Fig. 3a
10	300	800	800	800	800	5×10^{-13}	10^{-2}	0.1/0.3	10^{-3}	Fig. 3b
500	800	800	750	800	800	5×10^{-13}	10^{-3}	10^{-2}	10^{-3}	Fig. 3c
10	800	800	800	800	550	5×10^{-13}	10^{-3}	0.5/ 10^{-3}	$10^{-3}/0.02$	Fig. 3d

of dark matter that persists until the NLOP population fully decays. The resulting dark matter relic abundance is totally fixed from the NLOP's freeze-out density:

$$\Omega_{N_1}^{\text{super-WIMP}} = \frac{m_{N_1}}{m_{\text{NLOP}}} \Omega_{\text{NLOP}}^{\text{freeze-out}}. \quad (14)$$

This production mechanism is illustrated in Fig. 3, which showcases several distinct realizations of the NLOP within our model.

Figs. 3a and 3b depict scenarios where the NLOP is the fermionic state N_2 . Its freeze-out is driven by annihilations into SM leptons, mediated by the Yukawa couplings $(y_\Phi)_{a2}$ or $(y_\chi)_{a2}$. However, as shown in [62], LFV constraints severely limit $(y_\Phi)_{a2}$, suppressing the annihilation cross section and leading to an overproduction of N_2 if this coupling dominates. To achieve the correct relic abundance, additional mechanisms are required. One such mechanism is coannihilation: when N_2 is nearly degenerate in mass with other Z_2 -odd states, their com-

bined interactions enhance the effective annihilation rate. Fig. 3a compares two benchmarks: $m_{N_2} = 600$ GeV and 770 GeV, with the other odd particles fixed at 800 GeV. The heavier N_2 case benefits from stronger coannihilation effects, yielding a reduced freeze-out abundance consistent with observations. Alternatively, in our model, the coupling $(y_\chi)_{a2}$ opens an additional t -channel annihilation via exchange of the scalar singlet χ , producing neutrino final states. As demonstrated in Fig. 3b, increasing $(y_\chi)_{a2}$ significantly enhances the annihilation rate, lowering $\Omega_{N_2}^{\text{freeze-out}}$ and bringing the final dark matter density into agreement with cosmological data.

In scenarios where the scalar doublet Φ serves as the NLOP, we focus on its neutral real component ϕ_R as the representative case (with ϕ_I and ϕ^\pm exhibiting similar dynamics). ϕ_R annihilates efficiently through electroweak gauge interactions (e.g., $\phi_R \phi_R \rightarrow W^+ W^-, ZZ$), resulting in strong thermal coupling. The correct relic abundance is only achieved in mass region of $m_{\phi_R} > 500$ GeV (or $m_{\phi_R} < m_W$) [68–71]. In Fig. 3c, we consider a benchmark

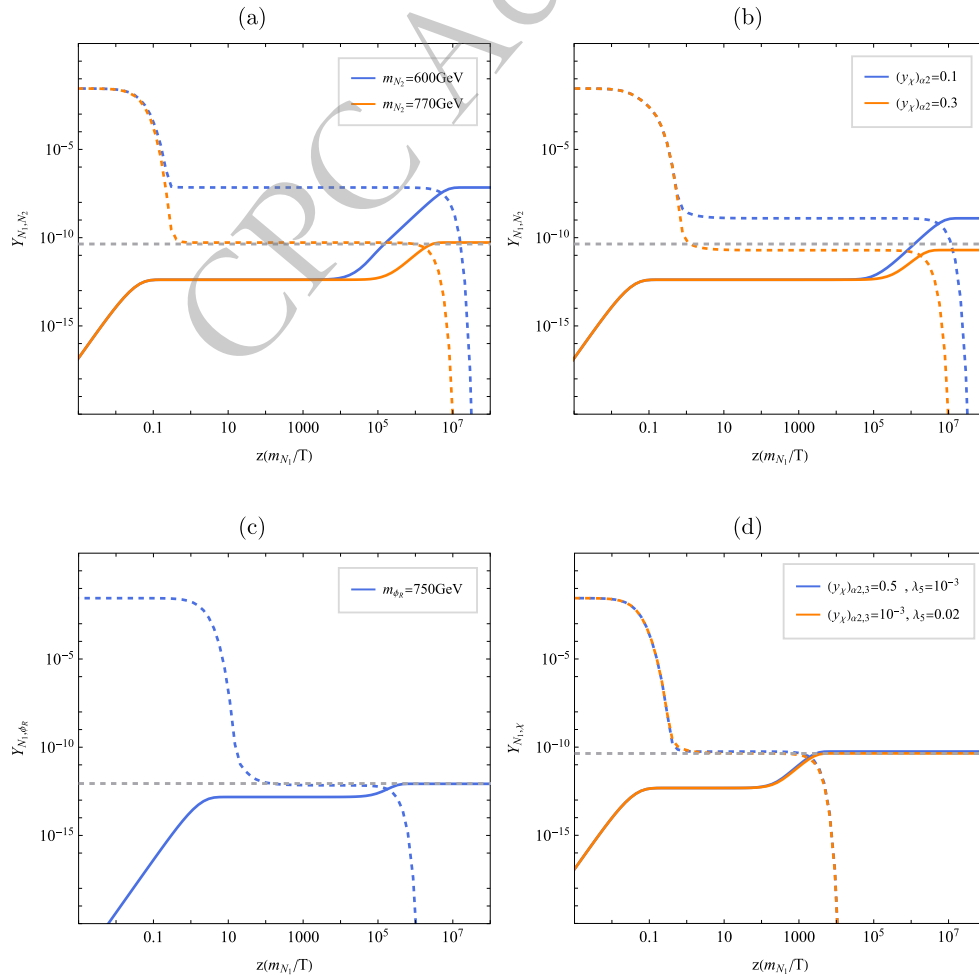


Fig. 3. (color online) The evolution of dark matter and NLOP under the "super-WIMP" mechanism. N_2 is chosen as NLOP in the upper two subfigures, while in the lower two subfigures ϕ_R and χ are selected as NLOP, respectively. The parameters used are listed in Table 2.

mass $m_{\phi_R} = 750$ GeV. A moderate mass hierarchy between N_1 and ϕ_R is required (hence we set $m_{N_1} = 500$ GeV), as the freeze-out abundance of ϕ_R is typically not significantly larger than the observed dark matter density [62].

For completeness, we also consider the phenomenology of the charged component ϕ^\pm when it acts as the NLOP. Being electrically charged and long-lived (due to suppressed decays into N_1), ϕ^\pm behaves as a long-lived charged particle. The ATLAS Collaboration has recently searched for such states in 140 fb^{-1} of pp collision data at $\sqrt{s} = 13$ TeV, using signatures based on high specific ionization energy loss and time-of-flight measurements [72]. Interpreting their results in the context of stau-to-gravitino decays, ATLAS excludes masses up to 560 GeV for such long-lived charged particles. Furthermore, in Fig. 4 we give the assessment of the projected sensitivity of future long-lived particle detector MATHUSLA [73]. Fig. 4 shows the projected reach in the mass-decay length plane of a long-lived ϕ^\pm [73], assumed to be pair-produced via Drell-Yan processes at the 14 TeV HL-LHC and to decay into dark matter. The reconstruction efficiency is assumed in 0.5–1. Contours indicate regions where at least four events are expected with 3 ab^{-1} . In Fig. 4 we also show the Yukawa coupling strength as a function of mass and decay length. Nevertheless, for the parameter space that yields the correct dark matter relic density, MATHUSLA's projected coverage remains limited to only a marginal segment.

Finally, we consider the scenario in which the scalar singlet χ serves as the NLOP. The annihilation of χ in the early universe is governed by three key parameters: the Yukawa coupling y_χ , the Higgs portal coupling λ_5 , and

the trilinear scalar coupling μ . Annihilation through y_χ proceeds via t -channel exchange of the heavy neutral fermions $N_{2,3}$, yielding neutrino final states. Alternatively, χ can annihilate into SM particle pairs—such as $b\bar{b}$, WW , or ZZ —through s -channel Higgs exchange, mediated by the $\lambda_5(H^\dagger H)\chi^2$ interaction. Motivated by the requirement of naturally small neutrino masses and the preservation of an approximate global symmetry in the scalar sector, we treat the coupling μ as hierarchically suppressed throughout this analysis. This naturalness argument renders μ negligible for thermal processes, leaving y_χ and λ_5 as the dominant drivers of χ 's annihilation dynamics. To illustrate the viable parameter space, we examine two representative benchmark scenarios. The first features a large Yukawa coupling $(y_\chi)_{2,3} = 0.5$ with a small Higgs portal $\lambda_5 = 10^{-3}$, favoring annihilation into neutrinos. The second adopts a larger portal coupling $\lambda_5 = 0.02$ while keeping $(y_\chi)_{2,3} = 10^{-3}$ small, enhancing annihilation into SM states via Higgs mediation. As shown in Fig. 3d, both configurations yield a χ freeze-out abundance that, after subsequent decay into N_1 , reproduces the observed dark matter relic density. This demonstrates the flexibility of the singlet χ NLOP scenario in achieving the correct dark matter yield through distinct but equally viable annihilation pathways.

IV. CONSTRAINTS FROM N_{eff}

The Dirac nature of neutrinos necessitates both left-handed (ν_L) and right-handed (ν_R) chiral components. The existence of ν_R contributes additional relativistic degrees of freedom, thereby increasing the radiation energy density in the early universe. This contribution is commonly parameterized by the effective number of relativistic species, defined as

$$N_{\text{eff}} = \frac{8}{7} \left(\frac{11}{4} \right)^{4/3} \frac{\rho_{\nu_L} + \rho_{\nu_R}}{\rho_\gamma} = 3 \left(\frac{11}{4} \right)^{4/3} \times \left[\left(\frac{T_{\nu_L}}{T_\gamma} \right)^4 + \left(\frac{T_{\nu_R}}{T_\gamma} \right)^4 \right]. \quad (15)$$

Within the SM, the effective number of relativistic species is precisely calculated to be $N_{\text{eff}}^{\text{SM}} = 3.045$ [74–76], incorporating effects from neutrino oscillations, non-thermal spectral distortions, and finite-temperature corrections. Any deviation from this value due to physics beyond the Standard Model (BSM) is typically expressed as $\Delta N_{\text{eff}} \equiv N_{\text{eff}} - N_{\text{eff}}^{\text{SM}}$. The Planck2018 results provide the most accurate and stringent constraint to date, yielding $\Delta N_{\text{eff}} \leq 0.285$ at the 2σ confidence level [77]. While the upcoming CMB-S4 experiment is projected to significantly improve sensitivity, with a forecasted reach of $\Delta N_{\text{eff}} \leq 0.06$ at the same confidence level [78].

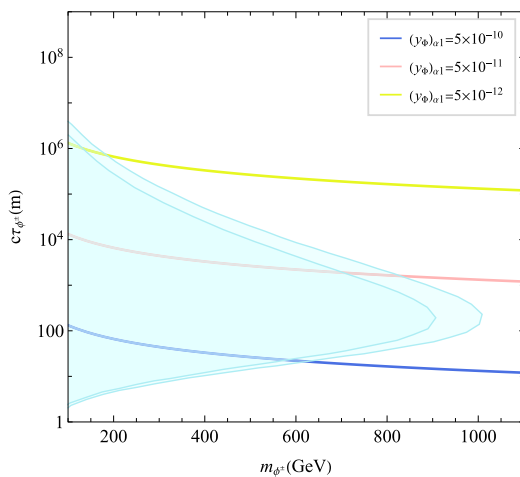


Fig. 4. (color online) The projected detecting capabilities of MATHUSLA to a long-lived ϕ^\pm , in the mass-decay length plane. The band shows the efficiencies vary from 0.5 to 1. Colored lines correspond to different strengths of Yukawa coupling between ϕ^\pm and the dark matter.

A. Thermal Contribution

In the early hot universe, all particles except the FIMP N_1 were in thermal equilibrium with the SM plasma. As the universe expanded and cooled, the dark plasma—comprising the scalar singlet χ , fermion singlets $N_{2,3}$, and right-handed neutrinos ν_R —gradually decoupled from the SM plasma. However, partial thermal equilibrium was maintained within the dark plasma due to the large Yukawa coupling y_χ . Interactions between the dark plasma and the SM plasma can occur through either $N_{2,3}$ or χ . For $N_{2,3}$, interactions with the SM are mediated by the coupling y_Φ , with the scattering amplitude scaling as $|y_\Phi|^2$. In contrast, χ couples to the SM either via t -channel Higgs exchange or through a contact interaction with Higgs, with the scattering amplitude proportional to λ_5 . Due to stringent constraints from LFV, y_Φ is typically too small to support significant interactions. As a result, the dominant portal between the dark plasma and the SM is mediated by χ . When χ eventually decouples from the SM plasma, the temperature of the right-handed neutrinos ν_R begins to deviate from that of the SM thermal bath. The decoupling temperature T_{dec} is determined by the condition: $\Gamma_{\text{el}}(T_{\text{dec}}) = H(T_{\text{dec}})$, where $\Gamma_{\text{el}} \equiv \sum n_{\text{SM}} \langle \sigma v \rangle_{\chi \text{SM} \rightarrow \chi \text{SM}} / (m_\chi / T)$ denotes the effective elastic scattering rate between χ and SM particles, accounting for the number of scatterings required to transfer energy of order T . In Fig. 5, we show the ratio Γ_{el}/H as a function of temperature for different values of λ_5 . The dashed line, corresponding to $\Gamma_{\text{el}}/H = 1$, indicates the condition for decoupling. The temperature ratio T_{ν_R}/T_{SM} can be determined using entropy conservation:

$$\frac{T_{\nu_R}}{T_{\text{SM}}} = \left(\frac{g_{\text{DP}}^{*S}}{g_{\text{SM}}^{*S}} \bigg|_{T_{\text{dec}}} \frac{g_{\text{SM}}^{*S}}{g_{\text{DP}}^{*S}} \right)^{1/3}, \quad (16)$$

where g_X^{*S} denotes the effective number of relativistic de-

grees of freedom, with respect to entropy density, in the X plasma (with "DP" referring to the dark plasma). The evaluation at T_{dec} indicates that the ratio is set at the dark plasma decoupling temperature. The evolution of T_{ν_R}/T_{SM} is shown in Fig. 5 for different choices of the dark plasma decoupling temperature. The later the dark plasma decouples (which corresponds to a larger λ_5 , and ν_R is heated more efficiently by the SM plasma over a longer period), the higher temperature ratio we will arrive at. This finally results in a larger contribution to the effective number of relativistic species.

B. Non-thermal Contribution from Delayed Decay of NLOP

In addition to thermal contributions from ν_R , the delayed decay of the NLOP—particularly during the BBN or CMB epochs—can leave observable imprints on cosmological data. Several studies in the literature have examined the late decays of heavy relics into electron-positron pairs [79] or neutrinos [80], and constraints have been derived based on their effects on BBN, CMB anisotropies and spectral distortions. In our model, the NLOP candidates include N_2 , $\phi_{R,I}$, ϕ^\pm , and χ (The roles of ϕ_R and ϕ_I as the NLOP are entirely analogous, therefore the following discussion for ϕ_R as the NLOP applies equally to ϕ_I). Among these, N_2 and ϕ^\pm can decay into SM charged leptons. Exotic electromagnetic (EM) energy injection is tightly constrained by cosmology. CMB observations (e.g., Planck) limit such injection as it alters recombination and distorts temperature and polarization spectra, while COBE-FIRAS rules out spectral distortions from early injection. During BBN, excess energy disrupts light-element abundances, conflicting with observed D and ^4He . Long-lived N_2 and ϕ^\pm with lifetimes between 3×10^4 s and recombination are strongly disfavored unless nearly degenerate with the dark matter

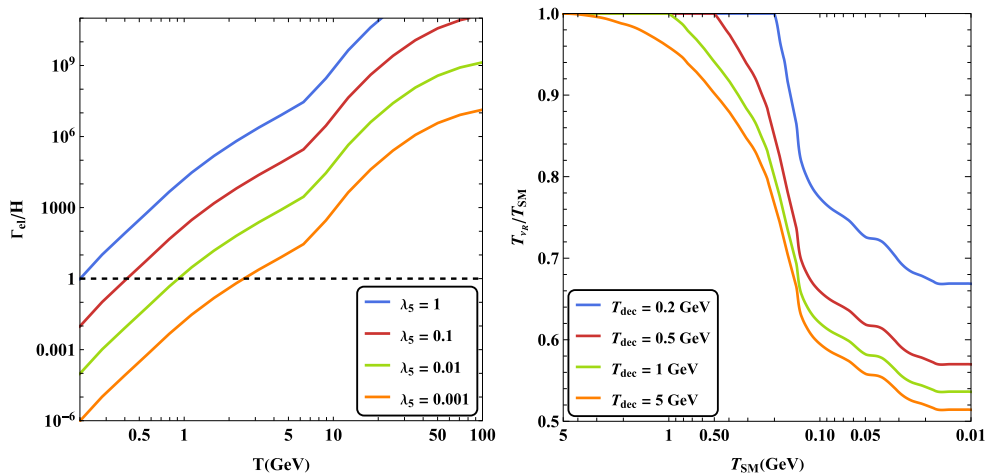


Fig. 5. (color online) (Left panel) The ratio of Γ_{el}/H as a function of temperature for different choice of λ_5 . Here we have chosen $m_\chi = 100$ GeV for demonstration. (Right panel) The evolution of ratio T_{ν_R}/T_γ for different dark plasma decoupling temperature.

(hence minimizing energy release) [79, 81–83]. In this work, we impose a conservative upper bound, requiring the lifetimes of N_2 and ϕ^\pm to be less than 3×10^4 s. For scenarios in which ϕ_R or χ is the NLOP, their delayed decays can inject energy into the left- or right-handed neutrinos, thereby altering the neutrino temperatures. The evolution of T_{ν_L} , T_{ν_R} , and T_γ is governed by the following system of differential equations:

$$\begin{aligned} \frac{dT_{\nu_L}}{dt} &= -HT_{\nu_L} + \frac{\delta\rho_{\nu_L} + \varepsilon_{\text{NLOP}}^{\nu_L} \frac{\rho_{\text{NLOP}}}{\tau_{\text{NLOP}}}}{3 \frac{\partial\rho_{\nu_L}}{\partial T_{\nu_L}}}, \\ \frac{dT_{\nu_R}}{dt} &= -HT_{\nu_R} + \frac{\varepsilon_{\text{NLOP}}^{\nu_R} \frac{\rho_{\text{NLOP}}}{\tau_{\text{NLOP}}}}{3 \frac{\partial\rho_{\nu_R}}{\partial T_{\nu_R}}}, \\ \frac{dT_\gamma}{dt} &= -\frac{4H\rho_\gamma + 3H(\rho_e + p_e) + \frac{\delta\rho_{\nu_L}}{\delta t}}{\frac{\partial\rho_\gamma}{\partial T_\gamma} + \frac{\partial\rho_e}{\partial T_\gamma}}. \end{aligned} \quad (17)$$

Here, ρ and p denote energy and pressure densities, respectively. ρ_{NLOP} stands for the energy density of NLOP, it evolves as

$$\frac{d\rho_{\text{NLOP}}}{dt} = -3H\rho_{\text{NLOP}} - \frac{\rho_{\text{NLOP}}}{\tau_{\text{NLOP}}}. \quad (18)$$

$\delta\rho/\delta t$ in Eq. 17 represents the energy transfer rate between the SM neutrinos and EM plasma due to weak interactions, as detailed in Refs. [84, 85]. The parameter $\varepsilon_{\text{NLOP}}^{\nu_L(\nu_R)} = (m_{\text{NLOP}}^2 - m_{N_1}^2)/(2m_{\text{NLOP}}^2)$ quantifies the fraction of the decaying NLOP's rest energy that is effectively deposited into $\nu_L(\nu_R)$ ¹. The initial conditions for this system are set at a time when ν_L and the photon bath were in thermal equilibrium ($T_{\nu_L} = T_\gamma$), and the NLOP has not yet decayed. In practice, we begin the numerical calculation at $T_\gamma = 10$ MeV, where ν_L is still coupled to the EM plasma, and any decays occurring earlier would contribute negligibly to the entropy of ν_L or ν_R . The starting temperature of ν_R is fixed by Eq. 16 with setting $T_{\text{SM}} = 10$ MeV. Following Ref. [80], we define a dimensionless parameter $f_{\text{NLOP}} \equiv \Omega_{\text{NLOP}}/\Omega_{\text{DM}}$, where Ω_{NLOP} represents the hypothetical present-day relic abundance of the NLOP if it were stable. Consequently, the initial energy density of the NLOP in Eq. 18 can be expressed as a function of f_{NLOP} . In principle, a similar differential equation system should be solved for N_2 or ϕ^\pm as the NLOP. However, we have verified that the BBN and CMB con-

straints (i.e. $\tau < 3 \times 10^4$ s) ensure that any late-decay effects on ΔN_{eff} are negligible.

We show the evolution of T_{ν_L}/T_γ (solid lines) and T_{ν_R}/T_γ (dashed lines) in Fig. 6, where the first row corresponds to ϕ_R as the NLOP and the second row to χ as the NLOP. The input parameters for Eqs. (17) and (18) are the NLOP energy fraction f_{NLOP} , its lifetime τ_{NLOP} , and the temperature of the right-handed neutrino bath at $T_\gamma = 10$ MeV, denoted $T_{\nu_R,10}$. We illustrate how different choices of these parameters influence the resulting temperature ratios. In the first column, we fix $f_{\text{NLOP}} = 100$ and $T_{\nu_R,10} = 5$ MeV. The NLOP lifetimes are set to 10^5 s, 10^6 s, and 10^7 s for illustration. As the lifetime of $\phi_R(\chi)$ increases, the delayed decay injects energy into $\nu_L(\nu_R)$ at a later cosmic time, leading to a more pronounced heating effect on $\nu_L(\nu_R)$. In the second column, we fix $\tau_{\text{NLOP}} = 10^7$ s and $T_{\nu_R,10} = 5$ MeV, and vary $f_{\text{NLOP}} = 10, 100$, and 1000 . A larger $f_{\phi_R(\chi)}$ implies a higher relic density after freeze-out, resulting in greater energy injection into $\nu_L(\nu_R)$ once the decays are complete. In the third column, we examine the impact of varying $T_{\nu_R,10}$ on the temperature ratio evolution. When ϕ_R is the NLOP, its late decay does not affect the thermal history of ν_R , and hence there is no heating of ν_R . When χ is the NLOP, variations in $T_{\nu_R,10}$ do not influence T_{ν_L}/T_γ , since χ decays exclusively into ν_R . A higher $T_{\nu_R,10}$ results in a larger T_{ν_R}/T_γ at the completion of χ decay.

With the time-dependent temperatures T_{ν_L} , T_{ν_R} , and T_γ determined, ΔN_{eff} can be computed using Eq. (15). From Eq. (17), it follows that the energy injection from NLOP decay into ν_L or ν_R proceeds in an identical manner in both scenarios. As a result, the evolution of ΔN_{eff} is the same whether the NLOP is ϕ_R or χ . We present the resulting ΔN_{eff} in Fig. 7, where the three subfigures show the effects of varying τ_{NLOP} , f_{NLOP} , and $T_{\nu_R,10}$, respectively. The two dashed lines stand for the current experimental limits from Planck [77] and future detecting capability from CMB-S4 [78]. A longer NLOP lifetime or a larger f_{NLOP} leads to a more pronounced heating effect, resulting in a higher ΔN_{eff} . A hotter ν_R bath, originating from stronger and more prolonged interactions between the dark plasma and the SM plasma, also yields a larger ΔN_{eff} . For completeness, we also show the evolution of ΔN_{eff} in the scenario where the contribution from the late decay of the NLOP is negligible, as depicted in the final subfigure of Fig. 7. This occurs when either the NLOP abundance is small or the NLOP lifetime is sufficiently short. In this limit, ΔN_{eff} is dominated solely by the thermal contribution from the decoupled ν_R bath. As expected, a higher $T_{\nu_R,10}$ results in a larger ΔN_{eff} , since the ν_R s contribute more to the radiation density.

¹ A portion of the energy injected into ν_L is subsequently transferred to photons and e^\pm via weak interactions, contributing to the thermalization of the EM plasma. The corresponding energy transfer fraction, denoted as ξ_{EM} in Ref. [80], can be read from Figure 1 of that work. For NLOP masses around the electroweak scale, ξ_{EM} is highly suppressed and effectively negligible. Therefore, we neglect this energy transfer in our analysis.

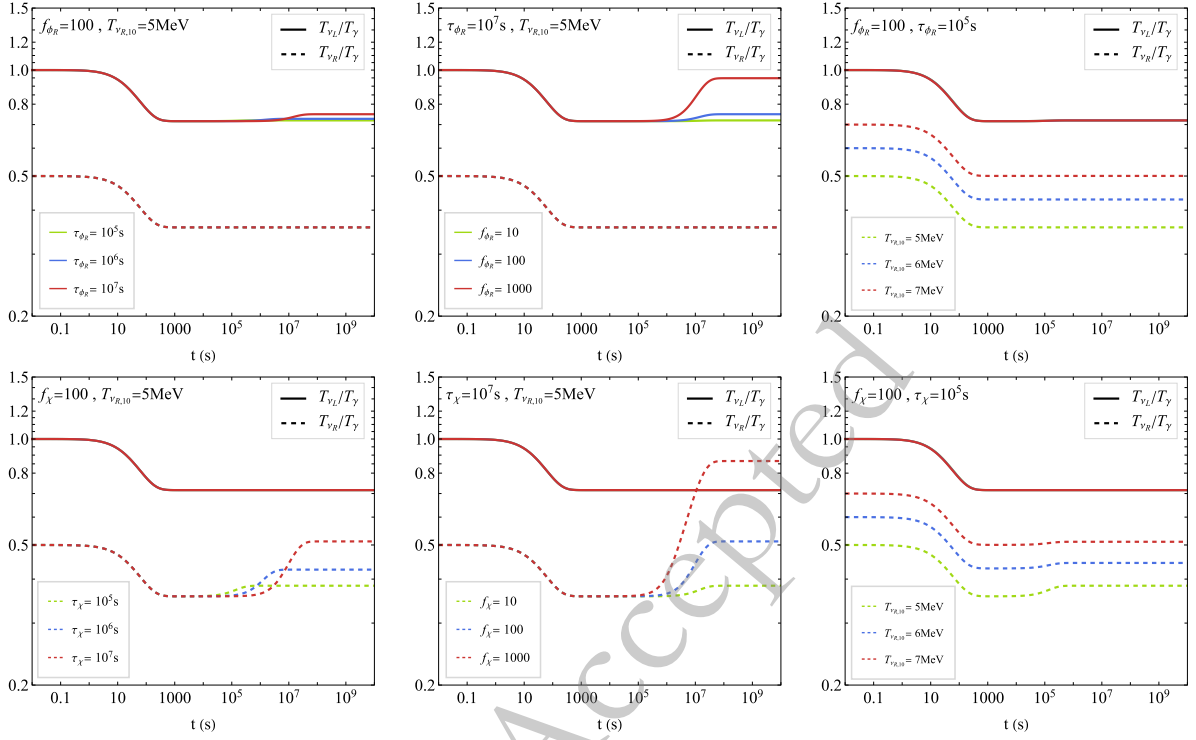


Fig. 6. (color online) The evolution of the temperature ratios T_{ν_L}/T_γ (solid lines) and T_{ν_R}/T_γ (dashed lines). The upper panel shows the case where ϕ_R is the NLOP, and the lower panel shows the case where χ is the NLOP.

C. Combined Results

Finally, we perform a comprehensive scan over the full parameter space, imposing constraints from dark matter relic density, neutrino mass, LFV, and cosmological observations such as BBN, CMB, and ΔN_{eff} . The scanning ranges for the model parameters are as follows:

$$\begin{aligned}
 m_{N_1} &\in [1, 1000] \text{ GeV}, & m_{\text{NLOP}} &\in [m_{N_1}, 1000] \text{ GeV}, \\
 m_{\text{others}} &\in [m_{\text{NLOP}}, 2000] \text{ GeV}, & (y_{\Phi, \chi})_{\alpha 1} &\in [10^{-15}, 10^{-7}], \\
 (y_{\Phi})_{\alpha 2,3} &\in [10^{-5}, 10^{-2}], & (y_{\chi})_{\alpha 2,3} &\in [10^{-3}, 1], \\
 \lambda_5 &\in [10^{-3}, 1], & \sin 2\theta &\in [10^{-10}, 10^{-5}].
 \end{aligned}
 \tag{19}$$

Here m_{NLOP} is the mass of the NLOP, and m_{others} refers to the masses of heavier odd-sector states. The lower bound on m_{ϕ^\pm} is set to 560 GeV, based on collider searches for long-lived charged particles [72]. The dark matter relic density is required to lie within the 3σ range of the Planck2018 measurement [77], i.e., $\Omega_{N_1} h^2 \in [0.117, 0.123]$. The odd states masses are scanned up to energy scale within reach of current and near-future experiments. The couplings $(y_{\Phi, \chi})_{\alpha 1}$ are bounded from above to ensure that dark matter remains out of thermal equilibrium. The couplings $(y_{\Phi})_{\alpha 2,3}$ are constrained by LFV bounds to be less than 10^{-2} , while $(y_{\chi})_{\alpha 2,3}$ are chosen to reproduce observed neutrino

masses. The mixing parameter $\sin 2\theta$ is restricted to below 10^{-5} on naturalness grounds—since $\theta = 0$ (or equivalently $\mu = 0$) enhances the model's symmetry. The quartic coupling λ_5 is scanned down to 10^{-3} , as the thermal contribution to ΔN_{eff} is no longer significant for smaller values.

As discussed in the previous subsection, we impose a conservative upper limit of $\tau < 3 \times 10^4 \text{ s}$ on the lifetime of the NLOP when it is either the charged scalar ϕ^\pm or the neutral fermion N_2 . This bound arises because EM energy injection from late decays can alter light element abundances during BBN and distort CMB anisotropies. However, when the NLOP is the neutral scalar ϕ_R , the constraints are significantly relaxed, as its dominant decays inject energy primarily into neutrinos rather than the EM plasma. In this case, we adopt the bounds from Ref. [80], which depend on the effective energy transfer parameter $f_{\phi_R} \mathcal{E}_{\phi_R}$, and display them as the blue curve in Fig. 8. In the scan, parameter points satisfying the dark matter relic density condition are colored pink. Among these, points that additionally satisfy constraints from neutrino mass and LFV processes are highlighted in green. Points that further pass the BBN and CMB bounds are shown in red. One can observe that the BBN and CMB limits exclude long-lived ϕ_R with lifetimes $\gtrsim 10^4$ – 10^7 s , although the constraints weaken significantly when the energy transferred to the neutrino sector is small. When the NLOP is the scalar χ , which decays directly into right-handed neutrino, there are no direct BBN or CMB con-

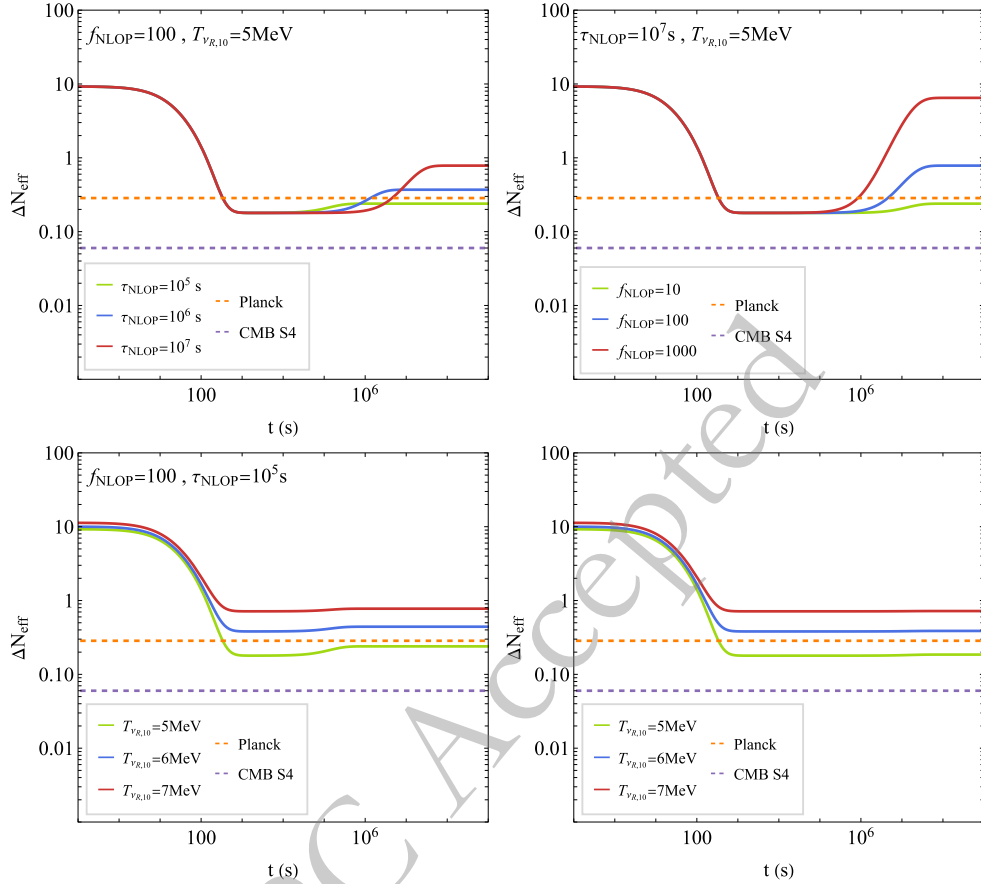


Fig. 7. (color online) Evolution of ΔN_{eff} for varying τ_{NLOP} , f_{NLOP} , and $T_{\nu R,10}$. The final subfigure illustrates the scenario in which ΔN_{eff} is dominated by thermal contributions.

straints, as the decay products are sterile and do not interact with the thermal bath.

In Fig. 9, we present the scanning results in the $m_{\text{NLOP}}-m_{N_1}$ plane, considering different particles as the NLOP. Constraints from dark matter relic density, neutrino mass and LFV, BBN and CMB, and ΔN_{eff} are applied successively. The color coding follows the same progression as in Fig. 8. Finally, points that also satisfy the ΔN_{eff} constraint are marked in blue, indicating full consistency with all observational requirements. The dark matter relic density receives contributions from both the freeze-in and super-WIMP mechanisms, as discussed in detail in Sect. III. Constraints from LFV, particularly the stringent experimental limit on the branching ratio of $\mu \rightarrow e\gamma$, exclude a significant portion of the parameter space. The impact of LFV constraints is also visible in the subfigure where χ is the NLOP, even though χ itself does not directly participate in LFV processes. This occurs because the same Yukawa couplings that govern LFV amplitudes also influence the dark matter production rate and thus must satisfy both relic density and flavor constraints simultaneously. The bounds from BBN and CMB have been discussed previously and are applied depending on the identity of the NLOP. In all cases—whether ϕ_R , χ , ϕ^\pm ,

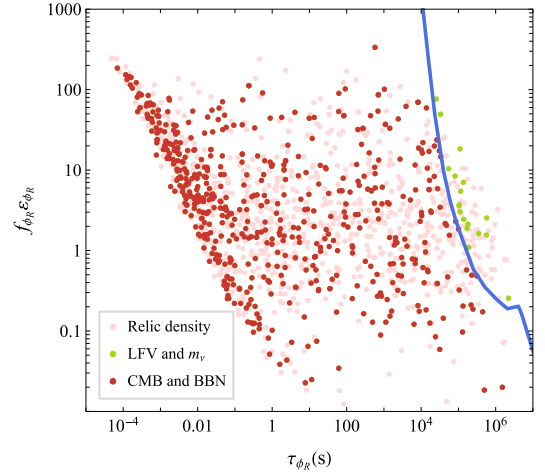


Fig. 8. (color online) Scan results in the $f_{\phi_R} \varepsilon_{\phi_R} - \tau_{\phi_R}$ plane for the case where ϕ_R is the NLOP. The blue curve shows the combined constraints from BBN and CMB as derived in Ref. [80].

or N_2 serves as the NLOP—we identify regions of parameter space that satisfy all observational constraints, including the latest limits on ΔN_{eff} . This demonstrates the viability of the FIMP Dirac scotogenic Model as a uni-

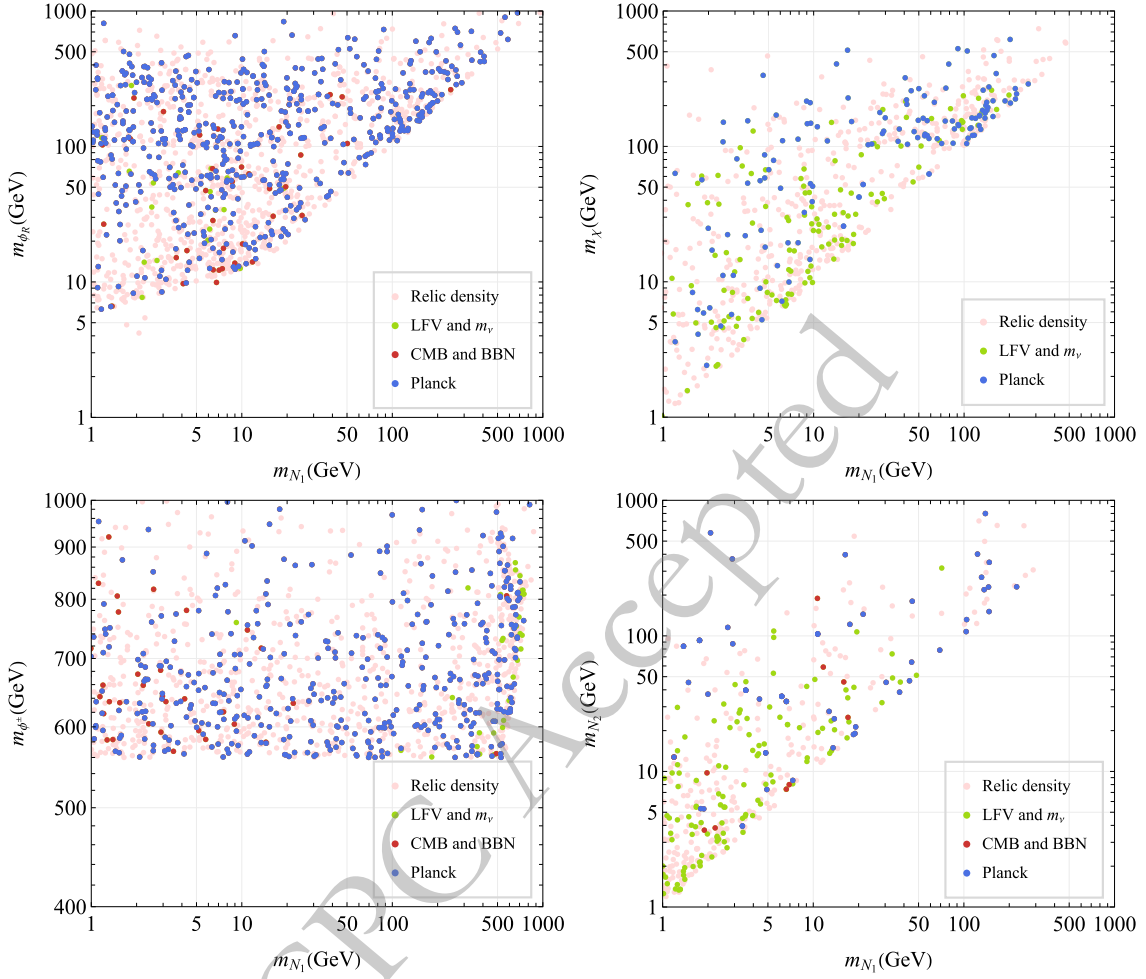


Fig. 9. (color online) Results of parameter scan in the $m_{N1} - m_{N2}$ plane under combined constraints from DM relic density, LFV, neutrino mass, CMB, BBN, and ΔN_{eff} .

fied framework for explaining both neutrino mass generation and the observed dark matter relic abundance. Future experiments will play a crucial role in testing this scenario. Long-lived particle searches at proposed facilities such as MATHUSLA [73] could probe the metastable NLOP states, while next-generation CMB observations from CMB-S4 [78] will improve sensitivity to ΔN_{eff} and energy injection during cosmic evolution. These experiments will either confirm the predictions of the model or further constrain its surviving parameter space.

V. CONCLUSION

In this work, we have studied the FIMP Dirac Scotogenic Model, a well-motivated extension of the SM that simultaneously addresses the origin of neutrino masses and the nature of dark matter. The lightest neutral fermion N_1 is a feebly interacting massive particle DM candidate, produced out of equilibrium. Neutrino masses are generated radiatively at one loop, resulting in a rank-2 mass matrix due to highly suppressed couplings to N_1 ,

predicting one nearly massless neutrino. Stringent LFV constraints, require the Yukawa couplings $(y_\Phi)_{\alpha 2,3}$ to be small, which in turn necessitates larger $(y_\chi)_{\alpha 2,3}$ to fit the neutrino mass scale. This coupling structure crucially impacts the phenomenology, governing the freeze-out dynamics of the NLOP and the thermal history of the right-handed neutrino bath.

We have systematically analyzed two distinct production mechanisms for N_1 : direct freeze-in via decays of heavier Z_2 -odd scalars and fermions, and the "super-WIMP" mechanism, where N_1 is produced from the late decay of a thermally frozen-out NLOP. The latter scenario leads to rich phenomenology, depending on whether N_2 , $\phi_{R,L}$, ϕ^\pm , or χ serves as the NLOP. We demonstrate that the correct relic abundance can be achieved across various benchmarks, with coannihilation effects and enhanced annihilation channels playing crucial roles in regulating the NLOP's freeze-out density, offering flexible pathways to match the observed DM density.

Another central focus of this work is the cosmological impact on the effective number of relativistic species.

Our analysis reveals two distinct contributions to this quantity. The first is a thermal contribution, arising from the primordial right-handed neutrino bath. This component is determined by the decoupling temperature of the ν_R bath, which is set by the strength of interactions between the dark sector and the SM plasma. The second contribution is non-thermal, originating from the late decays of the NLOP. The magnitude of this non-thermal contribution is highly sensitive to the NLOP's properties: both a longer lifetime τ_{NLOP} and a larger energy fraction f_{NLOP} lead to a more pronounced heating effect and thus a higher ΔN_{eff} .

We have performed a comprehensive parameter scan, sequentially applying constraints from DM relic density, neutrino mass and LFV, BBN/CMB, and ΔN_{eff} . Viable parameter space exists for all NLOP candidates that satisfy all current observational bounds. Future experiments setup for long-lived particle searches and precision ΔN_{eff} measurements will provide powerful probes to either discover this framework or further constrain its remaining parameter space.

Finally, It is instructive to contrast the two possible dark matter production mechanisms in our work: thermal freeze-out (WIMP) [63] versus freeze-in (FIMP). The distinction is most pronounced in the size of the Yukawa couplings $(y_{\Phi, \chi})_{\alpha 1}$ that govern the interaction of the lightest odd particle N_1 with the Standard Model sector. In the WIMP scenario, these couplings must be relatively large

to ensure efficient annihilation and avoid overproduction of dark matter. In the FIMP regime, by contrast, the couplings are extremely suppressed, $(y_{\Phi, \chi})_{\alpha 1} \lesssim 10^{-7}$, keeping N_1 out of thermal equilibrium throughout cosmic history. The relic density is then generated via the slow decay of heavier states, and this suppression naturally leads to a rank-2 neutrino mass matrix, predicting one nearly massless neutrino—a feature not generic in WIMP realizations. Phenomenologically, the two scenarios are also sharply distinguished by experimental constraints. WIMP parameter space is heavily constrained: collider searches exclude light dark matter masses, while direct and indirect detection experiments probe the TeV-scale region. In contrast, FIMPs evade these conventional probes due to their feeble couplings. Their collider signatures are limited to displaced decays of the NLOP (e.g., displaced vertices), and current long-lived particle searches provide only weak limits. Direct and indirect DM detection signals are negligible. Instead, the primary observational window for FIMPs lies in cosmology—particularly through their contribution to ΔN_{eff} from late decays of long-lived particles—which offers a powerful and complementary test of the freeze-in paradigm.

ACKNOWLEDGMENTS

We thank Zhi-Long Han, Ang Liu and Xiao-Dong Ma for helpful discussions.

References

- [1] R. Davis, J. r., D. S. Harmer, and K. C. Hoffman, *Phys. Rev. Lett.* **20**, 1205 (1968)
- [2] Y. Fukuda *et al.*, *Phys. Rev. Lett.* **81**, 1562 (1998), arXiv: hep-ex/9807003
- [3] F. P. An *et al.*, *Phys. Rev. Lett.* **108**, 171803 (2012), arXiv: 1203.1669
- [4] J. K. Ahn *et al.*, *Phys. Rev. Lett.* **108**, 191802 (2012), arXiv: 1204.0626
- [5] E. Aliu *et al.*, *Phys. Rev. Lett.* **94**, 081802 (2005), arXiv: hep-ex/0411038
- [6] Y. Abe *et al.*, *Phys. Rev. Lett.* **108**, 131801 (2012), arXiv: 1112.6353
- [7] Y. Cai, T. Han, T. Li, and R. Ruiz, *Front. in Phys.* **6**, 40 (2018), arXiv: 1711.02180
- [8] A. M. Sirunyan *et al.*, *JHEP* **01**, 122 (2019), arXiv: 1806.10905
- [9] M. J. Dolinski, A. W. P. Poon, and W. Rodejohann, *Ann. Rev. Nucl. Part. Sci.* **69**, 219 (2019), arXiv: 1902.04097
- [10] G. Anton *et al.*, *Phys. Rev. Lett.* **123**, 161802 (2019), arXiv: 1906.02723
- [11] N. Abgrall *et al.* (LEGEND) (2021), 2107.11462.
- [12] S. I. Alvis *et al.*, *Phys. Rev. C* **100**, 025501 (2019), arXiv: 1902.02299
- [13] E. Armengaud *et al.*, *Phys. Rev. Lett.* **126**, 181802 (2021), arXiv: 2011.13243
- [14] S. Abe *et al.*, *Phys. Rev. Lett.* **130**, 051801 (2023), arXiv: 2203.02139
- [15] C.-Y. Yao and G.-J. Ding, *Phys. Rev. D* **97**, 095042 (2018), arXiv: 1802.05231
- [16] S. Centelles Chuliá, R. Srivastava, and J. W. F. Valle, *Phys. Rev. D* **98**, 035009 (2018), arXiv: 1804.03181
- [17] J. Calle, D. Restrepo, C. E. Yaguna, and Ó. Zapata, *Phys. Rev. D* **99**, 075008 (2019), arXiv: 1812.05523
- [18] S. Jana, P. K. Vishnu, and S. Saad, *JCAP* **04**, 018 (2020), arXiv: 1910.09537
- [19] S. Saad, *Nucl. Phys. B* **943**, 114636 (2019), arXiv: 1902.07259
- [20] Y. Farzan and E. Ma, *Phys. Rev. D* **86**, 033007 (2012), arXiv: 1204.4890
- [21] P.-H. Gu and H.-J. He, *JCAP* **12**, 010 (2006), arXiv: hep-ph/0610275
- [22] P.-H. Gu and U. Sarkar, *Phys. Rev. D* **77**, 105031 (2008), arXiv: 0712.2933
- [23] S. Centelles Chuliá, E. Ma, R. Srivastava, and J. W. F. Valle, *Phys. Lett. B* **767**, 209 (2017), arXiv: 1606.04543
- [24] C. Bonilla, E. Ma, E. Peinado, and J. W. F. Valle, *Phys. Lett. B* **762**, 214 (2016), arXiv: 1607.03931
- [25] W. Wang and Z.-L. Han, *JHEP* **04**, 166 (2017), arXiv: 1611.03240
- [26] D. Borah and A. Dasgupta, *JCAP* **06**, 003 (2017), arXiv: 1702.02877
- [27] W. Wang, R. Wang, Z.-L. Han, and J.-Z. Han, *Eur. Phys. J. C* **77**, 889 (2017), arXiv: 1705.00414
- [28] S. Centelles Chuliá, R. Srivastava, and J. W. F. Valle, *Phys.*

- [Lett. B **773**, 26 \(2017\)](#), arXiv: [1706.00210](#)
- [29] E. Ma and U. Sarkar, *Phys. Lett. B* **776**, 54 (2018), arXiv: [1707.07698](#)
- [30] C.-Y. Yao and G.-J. Ding, *Phys. Rev. D* **96**, 095004 (2017), arXiv: [1707.09786](#)
- [31] C. Bonilla, J. M. Lamprea, E. Peinado, and J. W. F. Valle, *Phys. Lett. B* **779**, 257 (2018), arXiv: [1710.06498](#)
- [32] A. Ibarra, A. Kushwaha, and S. K. Vempati, *Phys. Lett. B* **780**, 86 (2018), arXiv: [1711.02070](#)
- [33] D. Borah and B. Karmakar, *Phys. Lett. B* **780**, 461 (2018), arXiv: [1712.06407](#)
- [34] A. Das, T. Nomura, H. Okada, and S. Roy, *Phys. Rev. D* **96**, 075001 (2017), arXiv: [1704.02078](#)
- [35] S. Centelles Chuliá, R. Srivastava, and J. W. F. Valle, *Phys. Lett. B* **781**, 122 (2018), arXiv: [1802.05722](#)
- [36] Z.-L. Han and W. Wang, *Eur. Phys. J. C* **78**, 839 (2018), arXiv: [1805.02025](#)
- [37] D. Borah, B. Karmakar, and D. Nanda, *JCAP* **07**, 039 (2018), arXiv: [1805.11115](#)
- [38] D. Borah and B. Karmakar, *Phys. Lett. B* **789**, 59 (2019), arXiv: [1806.10685](#)
- [39] C. D. R. Carvajal and Ó. Zapata, *Phys. Rev. D* **99**, 075009 (2019), arXiv: [1812.06364](#)
- [40] E. Ma, *Phys. Lett. B* **793**, 411 (2019), arXiv: [1901.09091](#)
- [41] A. Dasgupta, S. K. Kang, and O. Popov, *Phys. Rev. D* **100**, 075030 (2019), arXiv: [1903.12558](#)
- [42] K. Enomoto, S. Kanemura, K. Sakurai, and H. Sugiyama, *Phys. Rev. D* **100**, 015044 (2019), arXiv: [1904.07039](#)
- [43] S. Jana, P. K. Vishnu, and S. Saad, *Eur. Phys. J. C* **79**, 916 (2019), arXiv: [1904.07407](#)
- [44] E. Ma, *Eur. Phys. J. C* **79**, 903 (2019), arXiv: [1905.01535](#)
- [45] E. Ma, *Nucl. Phys. B* **946**, 114725 (2019), arXiv: [1907.04665](#)
- [46] D. Restrepo, A. Rivera, and W. Tangarife, *Phys. Rev. D* **100**, 035029 (2019), arXiv: [1906.09685](#)
- [47] S. Centelles Chuliá, R. Cepedello, E. Peinado, and R. Srivastava, *JHEP* **10**, 093 (2019), arXiv: [1907.08630](#)
- [48] J. Calle, D. Restrepo, and Ó. Zapata, *Phys. Rev. D* **101**, 035004 (2020), arXiv: [1909.09574](#)
- [49] R. Kumar, N. Nath, R. Srivastava, and S. Yadav (2025), 2505.01407.
- [50] Z. A. Borboruah, D. Borah, L. Malhotra, and U. Patel, *Phys. Rev. D* **112**, 015022 (2025), arXiv: [2412.12267](#)
- [51] B. De, D. Das, M. Mitra, and N. Sahoo, *JHEP* **08**, 202 (2022), arXiv: [2106.00979](#)
- [52] X. Luo, W. Rodejohann, and X.-J. Xu, *JCAP* **06**, 058 (2020), arXiv: [2005.01629](#)
- [53] X. Luo, W. Rodejohann, and X.-J. Xu, *JCAP* **03**, 082 (2021), arXiv: [2011.13059](#)
- [54] S. Centelles Chuliá, R. Srivastava, and S. Yadav, *JHEP* **04**, 038 (2025), arXiv: [2409.18513](#)
- [55] G. Arcadi, M. Dutra, P. Ghosh, M. Lindner, Y. Mambrini, M. Pierre, S. Profumo, and F. S. Queiroz, *Eur. Phys. J. C* **78**, 203 (2018), arXiv: [1703.07364](#)
- [56] Z. Bo *et al.*, *Phys. Rev. Lett.* **134**, 011805 (2025), arXiv: [2408.00664](#)
- [57] J. Aalbers *et al.*, *Phys. Rev. Lett.* **135**, 011802 (2025), arXiv: [2410.17036](#)
- [58] L. J. Hall, K. Jedamzik, J. March-Russell, and S. M. West, *JHEP* **03**, 080 (2010), arXiv: [0911.1120](#)
- [59] X. Liu, S.-Y. Guo, B. Zhu, and Y. Li, *Sci. Bull.* **67**, 1437 (2022), arXiv: [2204.04834](#)
- [60] L. Bian and X. Liu, *Phys. Rev. D* **99**, 055003 (2019), arXiv: [1811.03279](#)
- [61] A. G. Hessler, A. Ibarra, E. Molinaro, and S. Vogl, *JHEP* **01**, 100 (2017), arXiv: [1611.09540](#)
- [62] E. Molinaro, C. E. Yaguna, and O. Zapata, *JCAP* **07**, 015 (2014), arXiv: [1405.1259](#)
- [63] S.-Y. Guo and Z.-L. Han, *JHEP* **12**, 062 (2020), arXiv: [2005.08287](#)
- [64] K. Afanaciev *et al.* (MEG II) (2025), 2504.15711.
- [65] A. Alloul, N.-D. Christensen, C. Degrande, C. Duhr, and B. Fuks, *Comput. Phys. Commun.* **185**, 2250 (2014), arXiv: [1310.1921](#)
- [66] G. Alguero, G. Belanger, F. Boudjema, S. Chakraborti, A. Goudelis, S. Kraml, A. Mjallal, and A. Pukhov, *Comput. Phys. Commun.* **299**, 109133 (2024), arXiv: [2312.14894](#)
- [67] J. L. Feng, A. Rajaraman, and F. Takayama, *Phys. Rev. Lett.* **91**, 011302 (2003), arXiv: [hep-ph/0302215](#)
- [68] R. Barbieri, L. J. Hall, and V. S. Rychkov, *Phys. Rev. D* **74**, 015007 (2006), arXiv: [hep-ph/0603188](#)
- [69] L. Lopez Honorez, E. Nezri, J. F. Oliver, and M. H. G. Tytgat, *JCAP* **02**, 028 (2007), arXiv: [hep-ph/0612275](#)
- [70] M. Cirelli, N. Fornengo, and A. Strumia, *Nucl. Phys. B* **753**, 178 (2006), arXiv: [hep-ph/0512090](#)
- [71] T. Hambye, F. S. Ling, L. Lopez Honorez, and J. Rocher, *JHEP* **07**, 090 (2009), arXiv: [0903.4010](#)
- [72] G. Aad *et al.*, *JHEP* **07**, 140 (2025), arXiv: [2502.06694](#)
- [73] D. Curtin *et al.*, *Rept. Prog. Phys.* **82**, 116201 (2019), arXiv: [1806.07396](#)
- [74] G. Mangano, G. Miele, S. Pastor, T. Pinto, O. Pisanti, and P. D. Serpico, *Nucl. Phys. B* **729**, 221 (2005), arXiv: [hep-ph/0506164](#)
- [75] E. Grohs, G. M. Fuller, C. T. Kishimoto, M. W. Paris, and A. Vlasenko, *Phys. Rev. D* **93**, 083522 (2016), arXiv: [1512.02205](#)
- [76] P. F. de Salas and S. Pastor, *JCAP* **07**, 051 (2016), arXiv: [1606.06986](#)
- [77] N. Aghanim *et al.* (Planck), *Astron. Astrophys.* **641**, A6 (2020), [Erratum: *Astron. Astrophys.* 652, C4 (2021)], 1807.06209.
- [78] K. N. Abazajian *et al.* (CMB-S4) (2016), 1610.02743.
- [79] V. Poulin, J. Lesgourgues, and P. D. Serpico, *JCAP* **03**, 043 (2017), arXiv: [1610.10051](#)
- [80] T. Hambye, M. Hufnagel, and M. Lucca, *JCAP* **05**, 033 (2022), arXiv: [2112.09137](#)
- [81] M. Lucca, N. Schöneberg, D. C. Hooper, J. Lesgourgues, and J. Chluba, *JCAP* **02**, 026 (2020), arXiv: [1910.04619](#)
- [82] M. Kawasaki, K. Kohri, and T. Moroi, *Phys. Rev. D* **71**, 083502 (2005), arXiv: [astro-ph/0408426](#)
- [83] K. Jedamzik, *JCAP* **03**, 008 (2008), arXiv: [0710.5153](#)
- [84] M. Escudero, *JCAP* **02**, 007 (2019), arXiv: [1812.05605](#)
- [85] M. Escudero Abenza, *JCAP* **05**, 048 (2020), arXiv: [2001.04466](#)